

Imaging dynamically-driven strain at the nanometer-scale using stroboscopic Scanning X-ray Diffraction Microscopy

S. J. Whiteley,^{1,2} F. J. Heremans,^{1,3} G. Wolfowicz,^{1,4} D. D. Awschalom,^{1,3} and M. V. Holt⁵

¹*Institute for Molecular Engineering, University of Chicago, Chicago, Illinois 60637, USA*

²*Department of Physics, University of Chicago, Chicago, Illinois 60637, USA*

³*Institute for Molecular Engineering and Materials Science Division, Argonne National Laboratory, Argonne, Illinois 60439, USA*

⁴*WPI-Advanced Institute for Materials Research (WPI-AIMR), Tohoku University, Japan*

⁵*Center for Nanoscale Materials, Argonne National Laboratory, Argonne, Illinois 60439, USA**

(Dated: May 17, 2022)

Abstract

Phononic manipulation provides a direct route to control diverse materials properties in solid state systems. In materials hosting optically-active defects, strain control near engineered structures is an important path to harnessing the potential of solid-state qubits for quantum information science and nanoscale sensing. While lattice strain can be used both statically and dynamically to tune quantum energy levels and engineer hybrid system responses, the direct, independent observation of *in-situ* nanoscale strain fields induced near quantum defects remains challenging. We report the development of a stroboscopic Scanning X-ray Diffraction Microscopy (s-SXDM) imaging approach for investigating dynamic strain in 4H-SiC, which hosts vacancy related spin defects for quantum sensing and information. This approach uses nano-focused X-ray photon pulses synchronized to a surface acoustic wave (SAW) launcher, in order achieve static time domain and phase sensitive Bragg diffraction imaging with nanoscale spatial resolution near an engineered acoustic-scattering object. We use this technique to simultaneously map near-surface microstructures and acoustically induced lattice curvatures generated by interdigitated transducers fabricated on 4H-SiC as well as corroborate the images with the photoluminescence response of optically-active defect in the SiC, sensitive to local piezoelectric effects. The nanofocused diffraction patterns, stroboscopically varying in time, are analyzed to reveal micro-radian dynamic curvature oscillations trapped near a model structural defect etched into the SiC. This technique yields 0.01 pm d-spacing sensitivity and an effective time resolution of ~ 100 ps. These results demonstrate a unique route for directly studying local strain induced by acoustically manipulated structures under realistic operating conditions.

* mvholt@anl.gov

Strain provides a fundamental route to control diverse material properties such as transport [1], chemical reactivity [2], and electromagnetic ordering [3]. In quantum systems, the manipulation of strain near isolated point defects and engineered structures has shown the potential to significantly improve performance characteristics of solid-state qubits for quantum information processing [4–8]. Among potential degrees of freedom, mechanical coupling has the ability to nearly universally interact with solid-state realizations of quantum objects without introducing stray electromagnetic fields [9, 10]. From this, mechanical systems have the potential to play a transformative role in quantum information transfer, but the degree and nature of strain coupling to local properties, such as degenerate energy levels are often not well understood [11, 12]. Quantifying this coupling is especially important in the time domain, where dynamic sources of strain such as resonant acoustic waves can be used to directly switch quantum spin states via magnetically forbidden spin transitions [13–15] and control the transmission of single electron currents between qubits [16, 17].

We report the development of a new approach to imaging dynamic bulk crystal strain using recent advances in nanoscale hard X-ray microscopy techniques at 3rd generation synchrotron sources, which have enabled the visualization of sub-picometer embedded crystal strain with nanometer scale spatial resolution [18]. Using Bragg diffraction contrast as a scattering mechanism, this approach gives access to femtometer atomic displacements ($\Delta c/c \sim 10^{-5}$) in crystalline materials with a real-space, in-plane spatial resolution given by a beam focus on the order of tens of nanometers and at depths from tens to hundreds of microns. By virtue of the high monochromaticity of the light, tuning the scattering specifically to the diffraction condition of the quantum host material allows a positive strain contrast signal uncontaminated by the presence of capping material, transducer layers, or electrodes. This ability to access far-from-surface lattice perturbations in complex systems is combined with an ultrafast pulsed X-ray illumination determined by the bunch structure of the synchrotron storage ring [19]. We investigate acoustic strain modulation using 20 picosecond rms X-ray pulses separated by tens of nanoseconds synchronized to a surface acoustic wave (SAW) excitation that penetrates microns into the surface. In conventional schemes, the synchrotron timing structure is used to synchronize an optical pump during pulsed stimulation of the sample (optical pump / X-ray probe measurements) [20]. Our measurement instead uses a frequency match of continuous radio frequency (RF) surface acoustic wave excitation to the ring time structure, in order to virtually slow or freeze periodic lattice fluctuations generated by a transducer fabricated on the 4H-SiC host material.

Silicon carbide has been shown to be a versatile and increasingly relevant material for quantum sensing and technological applications due to a rich variety of optically accessible defect structures controllable up to room temperature with exceptionally long (ms) coherence times [11, 21–23]. In comparison to diamond, SiC is available commercially on the wafer-scale with industrial growth processes established along with well understood micro and nanofabrication steps for the creation of electronic, mechanical, and optical functionality [24, 25]. As robust as SiC neutral divacancy ground state spins are for storing quantum information, their excited state electronic energy levels can be manipulated and split with small amounts of crystalline strain ($< 10^{-6}$) in the host material [12]. SAW phonons have been used to demonstrate quantum manipulation of defect electronic orbitals in diamond [26] and spin states in SiC [15]. For the first time this study demonstrates a local measurement of lattice perturbations created by a SAW near a fabricated microscale structural defect in SiC. We are currently developing the methods to use nano-focused coherent diffraction imaging techniques such as 3D Bragg Projection Ptychography [27], which has the potential to image dynamic strain in four dimensions near lattice defects.

STROBOSCOPIC X-RAY DIFFRACTION MICROSCOPY

Propagating and stationary SAWs have widespread usage in RF signal processing and electronics applications [28] and are typically realized using an interdigitated transducer (IDT) on a piezoelectric crystal surface. In this study we use a ~ 500 nm thick piezoelectric transduction layer of sputtered AlN on a 4H-SiC substrate with low film stress and fabricate an IDT to drive the SAWs. The IDT contains a Ti under-metal layer for both improved metal-AlN adhesion and X-ray fluorescence mapping. Considering that both 4H-SiC and AlN have isotropic Rayleigh wave velocities in their respective crystal planes we apply Gaussian geometries, inspired by Gaussian optics and electromagnetism, to the IDT so as to form a nearly diffraction limited SAW spot size [15]. Gaussian focusing provides increased acoustic power near the focus, which is useful for increasing phonon coupling in hybrid quantum systems while minimizing SAW diffraction losses in resonators. The Gaussian IDT is geometrically designed to have a 1.25λ spot size (SAW wavelength $\lambda = 19.03 \mu\text{m}$) and Guoy phase incorporated for the lowest order Hermite-Gauss mode. Additionally, the piezoelectric AlN film is etched away at the SAW beam waist where 3λ of electrodes are removed to expose a window. The purpose of the window is to remove extraneous microstructure in the 4H-SiC caused by the internal film stress in the AlN epilayer clamping the substrate surface. Inside the IDT array, there is a standing wave produced by constructive interference from each of the individually phase matched electrodes.

The diffraction microscopy experiment sketched in Figure 1 consists of 8 keV X-rays generated by the Advanced Photon Source focused to a 25 nm FWHM beam spot by an interlaced zone doubled Fresnel zone plate [29] at the Hard X-ray Nanoprobe operated by the Center for Nanoscale Materials, Argonne National Laboratory. The sample is aligned to the 4H-SiC [0004] diffraction condition and the zone plate is raster scanned in real space relative to the sample position using an optomechanical nanopositioning system, allowing differential scanning of the nanofocused X-ray beam across the sample volume (Fig. S2) [30]. The RF excitation for producing SAW phonons is matched to a multiple of the synchrotron storage ring frequency (~ 352 MHz). This creates Bragg diffraction from a virtually frozen wave curvature and strain that can be temporally swept by adjusting the relative phase of the RF signal generator to the synchrotron source (Fig. 1b). A second approach to phase sampling we employ is to add a small detuning ($f_{ring} - f_{SAW} = 1 \pm 0.05$ Hz) to the SAW frequency relative to the ring frequency, which causes the signal to beat and evolve in phase at the detuning frequency. The resulting slow, time varying diffraction allows the SAW oscillation amplitude to be efficiently and periodically sampled without adjusting the electronics. Both approaches yielded similar results as a measure of local lattice distortion amplitude (Fig. S7). Here, the data we present are acquired in stroboscopic (time-sampled) mode. The far-field diffraction patterns are sensitive to strain components along the diffraction condition and lattice curvature or slope. The two characteristic positions of high curvature on the Gaussian focused surface acoustic wave are marked as magenta and green dots in Fig. 1c. It is important to note that the directions of the lattice curvature gradient at the magenta and green points are mutually orthogonal, creating distinct oscillatory motions of the far-field diffraction patterns on the detector shown exaggerated in Fig. 1c. These diffraction pattern oscillations are maximized at a characteristic set of positions where the curvature gradient reaches a maxima along the wave - either inflection points of the SAW propagation (longitudinal lattice slope - magenta dot) or gradient maxima of the Gaussian focusing (transverse lattice slope - green dot).

Results of the s-SXDM measurement are shown in Figure 2. The IDT shown in Fig. 2a is aligned relative to the scanning directions using X-ray fluorescence (XRF) from the Ti under-metal layer of the Al patterned electrodes as in Fig. 2b. At each scanning position twenty images

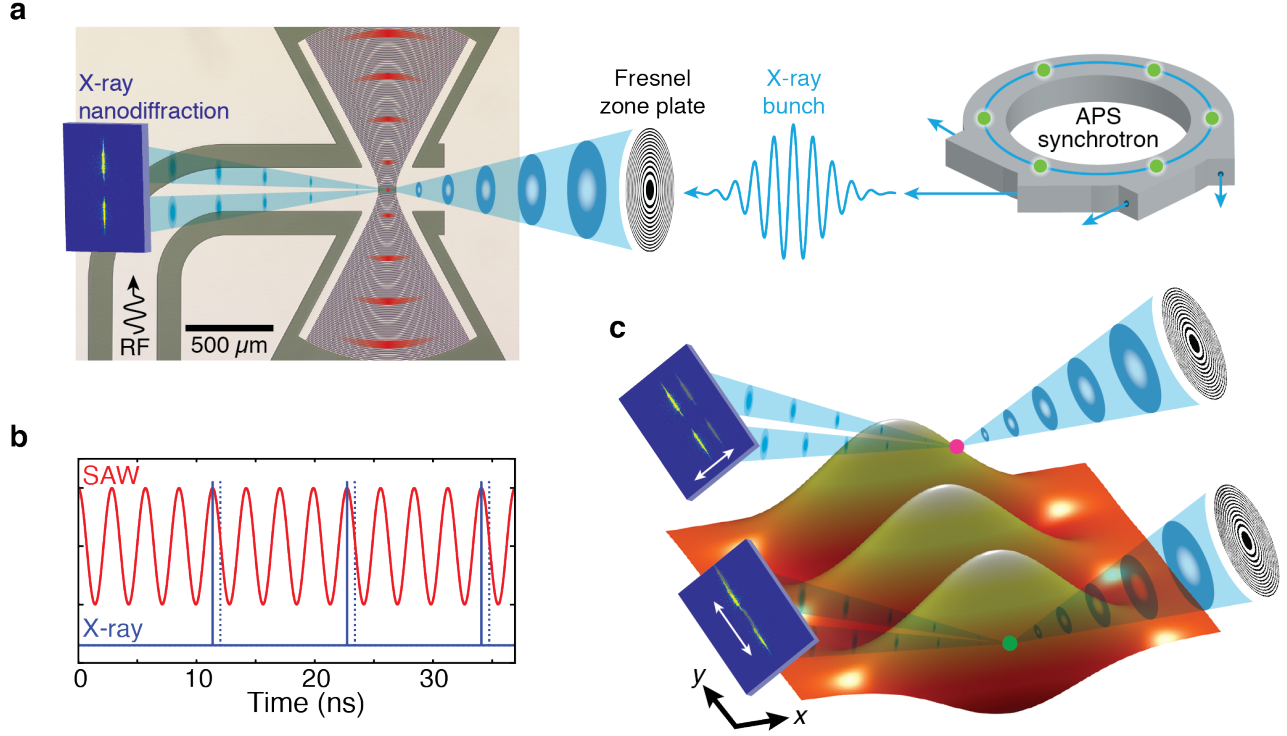


FIG. 1. Sketch of the stroboscopic Scanning X-ray Diffraction Microscopy (s-SXDM) experimental geometry. (a) Periodic bunch patterns of the Advanced Photon Source (APS) synchrotron are frequency matched to RF continuous wave excitation of a SAW (red). Stroboscopic illumination allows for nanoscale SXDM of a virtually frozen wave. (b) The time domain surface displacement of the SAW (red curve - 1 nm peak-to-peak displacement at 352 MHz) is synchronized to the time structure of the X-ray illumination (blue curve - 22 ps RMS width at 88 MHz). This allows a flexible measurement of the SAW amplitude by varying either time (detuned near-frequency match) or RF phase (at frequency match) to relatively displace the measurement to a new time slice (dotted blue line). (c) The out-of-plane displacement of the SAW at a fixed point in time is represented by the orange isosurface, exhibiting both periodic lattice curvature along the wave longitudinal propagation direction y and transverse curvature along x , at the magenta and green dots respectively, induced by Gaussian focusing of the standing wave. These curvatures induce orthogonal shifts in the far field diffraction pattern that oscillate as a function of the relative phase between the synchrotron time structure and the RF SAW excitation.

of the far field diffraction pattern are acquired at a 50 millisecond detector exposure time, allowing for full stroboscopic sampling. Oscillatory motions of the diffraction patterns are then separated into two components, one lying within the diffraction plane (x -axis) and one orthogonal to the diffraction plane (y -axis). These motions were primarily due to curvature inversion in the transverse and longitudinal (propagation) directions of the SAW, respectively. The images in Fig. 2c are calculated from peak-to-peak dynamic X-ray diffraction centroid shifts relative to the mean value at each position. This measure is used to remove spatially varying, time-independent lattice strain and curvature components in order to highlight SAW dynamics. Disorder visible in the longitudinal picture is primarily due to complex internal reflections from the AlN film windowing visible near the edges of both maps in Fig. 2c. Peak-to-peak displacement measurements fit to this curvature are consistent with a wave of ~ 1 nm surface displacement amplitude over a $10 \mu\text{m}$ half-period shown in Fig. 2d. The curvature is sampled along a $\sim 3 \mu\text{m}$ X-ray extinction length

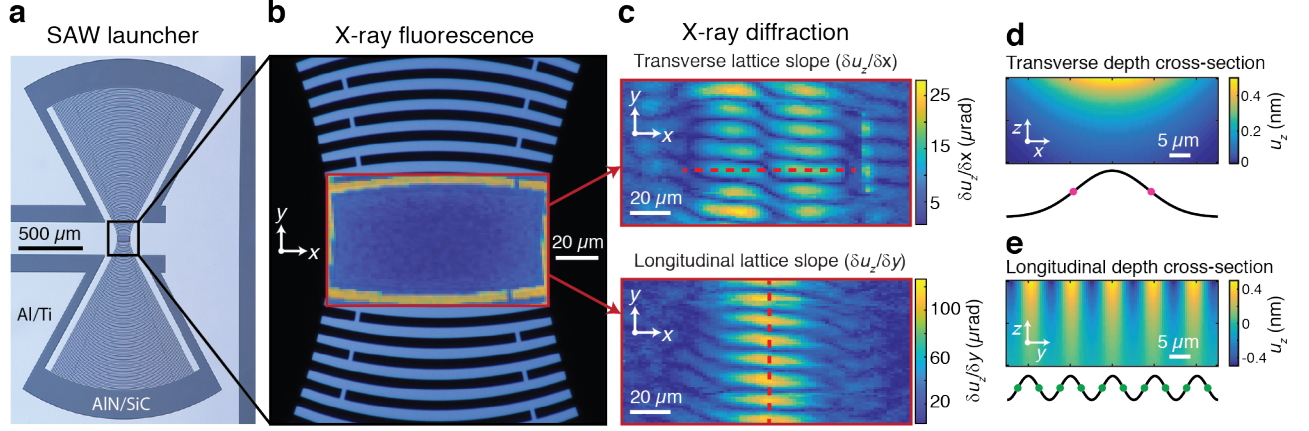


FIG. 2. Stroboscopic Scanning X-ray Diffraction Microscopy (s-SXDM) measurements made on a Gaussian SAW (a) with the wave propagation direction y aligned orthogonal to the scattering plane x . (b) The scanning X-ray Bragg diffraction measurements are registered relative to the patterned IDT using fluorescence from the Ti adhesion layer of the Al electrodes. (c) The far-field X-ray diffraction pattern is sensitive to the local curvature (tilt) of the lattice planes calculated as the gradient of the displacement in two ordinal components. The oscillatory transverse and longitudinal shifts of the X-ray diffraction pattern oscillation are independently detected as peak-to-peak displacements in the centroid position spot relative to the X-ray scattering plane. (d,e) The expected depth dependence of an ideal Gaussian surface acoustic wave displacement (u_z) along the transverse x (d) and longitudinal y (e) directions at the dashed red lines in (c). The transverse (longitudinal) curvature maxima, signified with magenta (green) dots, correlate with the double (single) lobed periodic features, respectively, experimentally observed in (c). The calculated displacements correspond to the experimentally observed curvature amplitude.

expected at the [0004] reflection oriented at a scattering angle of $\approx 18^\circ$, resulting in a $1 \mu\text{m}$ depth sampling of the transverse and longitudinal curvature fluctuations. No fluctuations are measured when the SAW power was reduced to zero (Fig. S6).

IMAGING STRUCTURAL DEFECTS

In order to assess the local sensitivity of the s-SXDM method, we fabricate a structural defect into the center of the SiC scanning window (Fig. 3a) to perturb the Gaussian SAW. This structural defect consists of a pit dry etched ($\sim 2.7 \mu\text{m}$ diameter, $1 \mu\text{m}$ deep) into the SiC surface. The dynamic (time-dependent) strain perturbation of the etch pit in response to the acoustic wave is expected to be relatively large, as shown by a mechanical model in Fig. 3b. This effect can in principle be valuable for eliciting responses of nearby quantum defects, as it results in a locally enhanced strain and piezoelectric coupling response in the 4H-SiC, as simulated in Fig. 3c. We use native divacancy defect ensembles, which emit photoluminescence (PL) in the near-infrared, as local sensors for RF electric fields. By employing Electrometry by Optical Charge Conversion (EOCC), we all-optically map the defect ensemble responses to dynamic electric fields induced piezoelectrically. In this methodology, the optical charge conversion rates are sensitive to fluctuations in the local electric field (E^2), which we measure in the steady state by simultaneously illuminating the divacancy ensembles with both ultraviolet and near-infrared light [31]. We find that PL contrast during SAW excitation is spatially maximized near the structural defect (Fig. 3d).

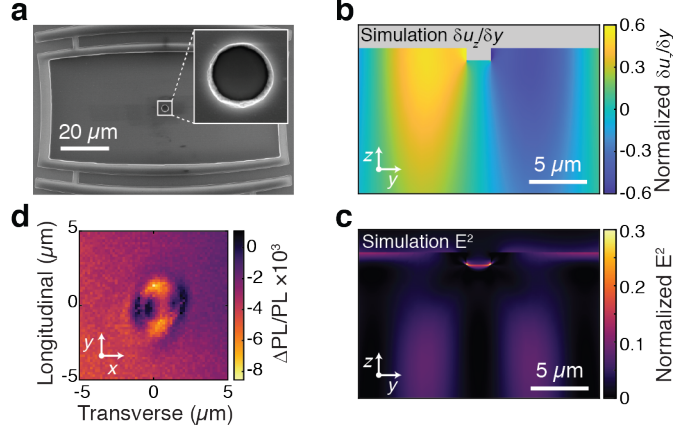


FIG. 3. Structural defect and internal piezoelectric response. (a) SEM image of model structural defect, an etched pit, located at the center of the SAW beam waist. (b-c) Simulated depth cross-section of the longitudinal lattice curvature and electric field magnitude (E^2) in the SiC substrate. The finite element models are computed using COMSOL Multiphysics and show a time slice during continuous RF excitation of the SAW. Although the etch pit is located at a node in longitudinal curvature, increased strain and piezoelectric effects happen at the pit's base and corners. (d) Enhanced dynamic piezoelectric effects at the pit are independently and all-optically mapped by native quantum defects using Electrometry by Optical Charge Conversion [31], which is sensitive to the local E^2 . Peaks of signal are visible at the longitudinal pit edges, and the background is from stray electric fields (see Fig. S4 for depth dependence of PL contrast).

These results suggests that internal dynamic strains, detected by electric fields in the piezoelectric bulk 4H-SiC, are strongly enhanced near the etch pit corners. Furthermore, the depth dependence of PL contrast from the divacancies (Fig. S4c) indicates that the dynamic strain and piezoelectric fields are located microns away from the SiC surface. This is in agreement with our numerical simulations (Fig. 3c) that reveal the linear strain amplitude near the structural defect base is over three times greater compared to strain from the propagating SAW amplitude alone.

We directly measure the dynamic transverse curvature amplitudes near the etch pit by s-SXDM (Fig. 4a). The expected instantaneous curvature of an unperturbed SAW is predicted with a simple phenomenological model assuming only Hermite-Gauss modes from the IDT. We find that an additional rotation degree of freedom relative to the scattering plane explains the weak S-shaped connections of the bimodal transverse curvature. This prediction is subtracted from the experimentally observed curvature amplitude in order to highlight the near-defect behavior, the results of which are shown in Fig. 4b. The etch pit is intended to create an outgoing secondary wave, or a local reflection of the wave which is weakly visible as patches of excess transverse amplitude and distortions of the longitudinal amplitude circularly surrounding the central position at a $\sim \lambda/2$ ($9.5\mu\text{m}$) radius.

Combining the nanometer-scale spatial resolution and stroboscopic feature of our X-ray imaging technique allows us to locally image both the static and actively driven lattice distortions around the etch pit. Static local strain induced by the dry etch process is relatively small and nonetheless can be directly visualized by the mean (time independent) diffraction pattern recorded at each scanning position (Fig. 4c,d). The static bound strain results can be understood as compressive (tensile) strain in the upper (lower) pit corners, respectively, which average and cancel each other when scanning through the center. At a higher degree of visibility in the dynamic variations (Fig. 4e) compared to an outgoing wave, and trapped within the diameter of the etch pit, we

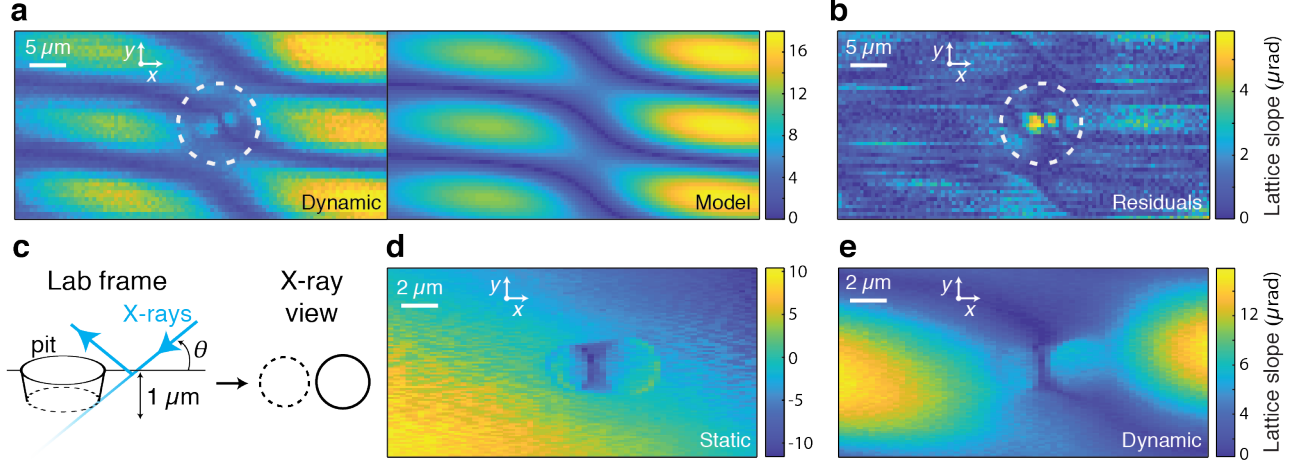


FIG. 4. Near structural defect dynamic curvature measured via s-SXDM. (a) (Left) Real - space maps of diffraction oscillation amplitude, grey circle show presence of the fabricated pit in the SiC surface. (Right) The expected instantaneous curvature predicted with a simple phenomenological model including Gaussian focusing and wave periodicity as free parameters. The weak S-shaped connection of the bimodal transverse curvature originates from a small (~ 2 deg) misalignment of the diffraction plane to the wave propagation direction. (b) The best fit of the model parameters were then used to subtract the curvature of the unperturbed SAW, allowing approximate visualization of the outgoing secondary wave and clear visualization of a locally trapped high amplitude wave near the pit (dashed circle). The spatial step size in (a,b) is 500 nm, with a 25 nm spot size. (c) SXDM sketch of the fabricated structural defect with a scattering angle $\Theta \approx 18$ degrees. The surface coordinate scanning is corrected for sample angle relative to X-ray beam. (d) Nanoscale imaging near the pit of static strain, or lattice curvature, from the mean x centroid shift. (e) Dynamic transverse curvature from the r.m.s. x centroid shift during stroboscopic imaging. The spatial step size in (d,e) is 50 nm, with a 25 nm spot.

observe a strong bimodal peak. By raster scanning the beam and correlating the resulting bound strain, we determine that this trapped acoustic feature is microns below the surface and varying in time, demonstrating the value of this synchrotron microscopy method as a local direct measurement of defect interactions with dynamic strain induced by acoustic wave. Such an effect could in principle be used to locally focus acoustics near quantum relevant defects within a nanostructure in order to achieve stronger time-varying distortions for state manipulation.

DISCUSSION

Surface acoustic waves have been previously observed with frequency-matched synchrotron X-ray diffraction, historically with diffraction micro-topography [32, 33], and more recently with iterative phase retrieval of surface structure using SAW satellite peaks [34, 35]. Here, we demonstrated nano-focused, direct-space Bragg diffraction microscopy using the synchrotron timing structure to stroboscopically image lattice curvature associated with a SAW. This new methodology enables three orders of magnitude higher spatial resolution versus previous topographic methods and access to independent ordinal components of lattice curvature and strain [36] rather than a single scalar projection of these quantities as in previous X-ray topographic studies. This is a necessary step towards the goal of simultaneous picosecond and nanoscale imaging of a single

defect interacting with resonant local phonons.

In summary, we imaged local, dynamic lattice perturbations induced by a Gaussian focused surface acoustic wave, interacting with a fabricated structural defect in 4H-SiC. This approach is based on the frequency matching of a synchrotron X-ray pulse structure to a RF transducer and makes use of nano-focused hard X-ray diffraction microscopy for real-space nanoscale strain imaging in the time domain. The induced strain and dynamic lattice fluctuations observed hold important consequences for quantum response engineering, as indicated by the preliminary photoluminescence contrast enhancement. A key feature enabled by this methodology is removing ambiguity in assessing quantum structure-function relationships, through the congruent ability to image in real-space lattice fluctuations that directly relate to photoluminescence changes from optically-active point defects. Beyond quantum materials, this method is generally applicable to acoustically manipulated structures where simultaneous picosecond time, nanoscale spatial, and sub-picometer strain displacement sensitivity can be used for unique local visualization of mechanical energy transduction.

METHODS

Sample Fabrication

The high purity semi-insulating 4H-SiC substrate from Cree Inc. had ~ 500 nm AlN sputtered by OEM Group Inc. onto the wafer Si-face with low film stress. The IDT, comprising of 20 nm thick Ti and 150 nm thick Al, was fabricated on the AlN/SiC substrate. The circular pit (Fig. 3a) was measured to be ≈ 950 nm deep by AFM using an Asylum Research Cypher S and the depth was also confirmed with laser confocal microscopy using an Olympus LEXT OLS5000. All layers were processed by optical lithography techniques and inductively coupled plasma etching. Extensive fabrication and device characterization details are shown in the supplementary materials.

-
- [1] W. Wu and Z. L. Wang, *Nature Reviews Materials* **1**, 16031 (2016).
 - [2] L. Oakes, R. Carter, T. Hanken, A. P. Cohn, K. Share, B. Schmidt, and C. L. Pint, *Nature Communications* **7**, 1 (2016).
 - [3] D. Sando, A. Agbelele, D. Rahmedov, J. Liu, P. Rovillain, C. Toulouse, I. C. Infante, J.-m. L. Breton, M. Cazayous, A. Sacuto, J. Juraszek, A. K. Zvezdin, L. Bellaiche, and B. Dkhil, *Nature Materials* **12**, 641 (2013).
 - [4] T. D. Ladd, F. Jelezko, R. Laflamme, Y. Nakamura, C. Monroe, and J. L. O. Brien, *Nature* **464**, 45 (2010).
 - [5] M. V. Gustafsson, T. Aref, A. F. Kockum, K. Maria, G. Johansson, and P. Delsing, *Science*, 1 (2014).
 - [6] F. J. Heremans, C. G. Yale, and D. D. Awschalom, *Proceedings of the IEEE* **104**, 2009 (2016).
 - [7] L. C. Bassett, F. J. Heremans, C. G. Yale, B. B. Buckley, and D. D. Awschalom, *Physical Review Letters* **107**, 266403 (2011).
 - [8] C. F. de las Casas, D. J. Christle, J. U. Hassan, T. Ohshima, N. T. Son, and D. D. Awschalom, *Appl. Phys. Lett.* **111**, 262403 (2017).
 - [9] G. Kurizki, P. Bertet, Y. Kubo, K. Mølmer, D. Petrosyan, and P. Rabl, *Proceedings of the National Academy of Sciences of the United States of America* **112**, 3866 (2015).

- [10] M. J. A. Schuetz, E. M. Kessler, G. Giedke, L. M. K. Vandersypen, M. D. Lukin, J. I. Cirac, and M.-p.-i. Quantenoptik, *Phys. Rev. X* **031031**, 1 (2015).
- [11] J. R. Weber, W. F. Koehl, J. B. Varley, A. Janotti, B. B. Buckley, C. G. Van de Walle, and D. D. Awschalom, *Proceedings of the National Academy of Sciences of the United States of America* **107**, 8513 (2010).
- [12] A. L. Falk, P. V. Klimov, B. B. Buckley, V. Ivády, I. A. Abrikosov, G. Calusine, W. F. Koehl, Á. Gali, and D. D. Awschalom, *Physical Review Letters* **112**, 187601 (2014).
- [13] A. Barfuss, J. Teissier, E. Neu, A. Nunnenkamp, and P. Maletinsky, *Nature Physics* **11**, 820 (2015).
- [14] E. R. Macquarrie, T. A. Gosavi, S. A. Bhawe, G. D. Fuchs, and W. Lafayette, *Physical Review B* **224419**, 1 (2015).
- [15] S. J. Whiteley, G. Wolfowicz, C. P. Anderson, A. Bourassa, H. Ma, M. Ye, G. Koolstra, K. J. Satzinger, M. V. Holt, F. J. Heremans, A. N. Cleland, D. I. Schuster, G. Galli, and D. D. Awschalom, submitted (2018).
- [16] F. J. R. Schüle, E. Zallo, P. Atkinson, O. G. Schmidt, R. Trotta, A. Rastelli, A. Wixforth, and H. J. Krenner, *Nature nanotechnology* **10** (2015), 10.1038/nnano.2015.72.
- [17] T. M. Sylvain Hermelin, Shintaro Takada, Michihisa Yamamoto, Seigo Tarucha, Andreas D. Wieck, Laurent Saminadayer, Christopher Bauerle, *Nature* **477**, 435 (2011).
- [18] M. Holt, R. Harder, R. Winarski, and V. Rose, *Annual Review of Materials Research* **43**, 183 (2013).
- [19] G. Shenoy, P. Viccaro, and D. Mills, *Characteristics of the 7-GeV advanced photon source: A guide for users* (1988).
- [20] J. N. Clark, L. Beitra, G. Xiong, A. Higginbotham, D. M. Fritz, H. T. Lemke, D. Zhu, M. Chollet, G. J. Williams, M. Messerschmidt, B. Abbey, R. J. Harder, A. M. Korsunsky, J. S. Wark, and I. K. Robinson, *Science* , 56 (2013).
- [21] W. F. Koehl, B. B. Buckley, F. J. Heremans, G. Calusine, and D. D. Awschalom, “Room temperature coherent control of defect spin qubits in silicon carbide,” (2011).
- [22] D. J. Christle, A. L. Falk, P. Andrich, P. V. Klimov, J. U. Hassan, N. T. Son, E. Janzén, T. Ohshima, and D. D. Awschalom, *Nature materials* **14**, 160 (2015).
- [23] M. Widmann, S.-Y. Lee, T. Rendler, N. T. Son, H. Fedder, S. Paik, L.-P. Yang, N. Zhao, S. Yang, I. Booker, A. Denisenko, M. Jamali, S. A. Momenzadeh, I. Gerhardt, T. Ohshima, A. Gali, E. Janzén, and J. Wrachtrup, *Nature materials* **14**, 164 (2015).
- [24] D. O. Bracher, X. Zhang, and E. L. Hu, *Proceedings of the National Academy of Sciences of the United States of America* **114**, 4060 (2017).
- [25] G. Calusine, A. Politi, D. D. Awschalom, G. Calusine, A. Politi, and D. D. Awschalom, *Applied Physics Letters* **105** (2014).
- [26] D. A. Golter, T. Oo, M. Amezcua, K. A. Stewart, and W. H, *Physical Review Letters* **116**, 143602 (2016).
- [27] S. O. Hruszkewycz, M. Allain, M. V. Holt, C. E. Murray, J. R. Holt, P. H. Fuoss, and V. Chamard, *Nature Materials* **16** (2017), 10.1038/NMAT4798.
- [28] C. Campbell, *Surface acoustic wave devices and their signal processing applications* (1989).
- [29] J. V. Comamala, A. Diaz, M. Guizar-Sicairos, A. Manton, C. M. Kewish, A. Menzel, O. Bunk, and C. David, *Optics Express* **19**, 21333 (2011).
- [30] R. P. Winarski, M. V. Holt, V. Rose, P. Fuesz, D. Carbaugh, C. Benson, D. Shu, D. Kline, G. B. Stephenson, I. McNulty, and J. Maser, *Journal of Synchrotron Radiation* **19**, 1056 (2012).
- [31] G. Wolfowicz, S. J. Whiteley, and D. D. Awschalom, *Proc. Natl. Acad. Sci.* (2018), 10.1073/pnas.1806998115.
- [32] R. W. Whatmore, P. A. Goddard, B. K. Tanner, and G. F. Clark, *Nature* **299**, 44 (1982).

- [33] E. Zolotoyabko, D. Shilo, and E. Lakin, *Materials Science and Engineering* **309-310**, 23 (2001).
- [34] T. Reusch, F. Schüle, C. Bömer, M. Osterhoff, A. Beerlink, H. J. Krenner, A. Wixforth, and T. Salditt, *AIP Advances* **072127** (2013).
- [35] J.-d. Nicolas, T. Reusch, M. Osterhoff, M. Sprung, H. J. Krenner, A. Wixforth, and T. Salditt, *Journal of Applied Crystallography* **47**, 1596 (2014).
- [36] M. V. Holt, S. O. Hruszkewycz, C. E. Murray, J. R. Holt, D. M. Paskiewicz, and P. H. Fuoss, *Phys. Rev. Lett.* **165502**, 1 (2014).

I. ACKNOWLEDGMENTS

The fabrication of the surface acoustic wave devices was supported by the Air Force Office of Scientific Research. The experimental design and surface acoustic wave microwave driving and synchronization was supported by the US Department of Energy, Office of Science, Basic Energy Sciences, Materials Sciences and Engineering Division. The SXDM measurements were performed at the Hard X-ray Nanoprobe Beamline operated by the Center for Nanoscale Materials, an Office of Science user facility, supported by the U.S. Department of Energy, Office of Science, Office of Basic Energy Sciences, under Contract No. DE-AC02-06CH11357. This work made use of shared facilities supported by the NSF MRSEC Program under DMR-0820054 and the Pritzker Nanofabrication Facility of the Institute for Molecular Engineering at the University of Chicago, which receives support from Soft and Hybrid Nanotechnology Experimental (SHyNE) Resource (NSF ECCS-1542205), a node of the National Science Foundations National Nanotechnology Coordinated Infrastructure. The authors thank Stephan O. Hruszkewycz, Paul C. Jerger, Brian B. Zhou and Paul Evans for careful reading of the manuscript.